EUROGRAPHICS 2004 / M.-P. Cani and M. Slater
(Guest Editors)

Volume 23 (2004), Number 3

Topological Construction and Visualization of Higher Order 3D Vector Fields

T. Weinkauf[1], H. Theisel[2], H.-C. Hege[1] and H.-P. Seidel[2]

[1] Zuse Institute Berlin (ZIB), Berlin, Germany — {weinkauf, hege}@zib.de
[2] MPI Informatik, Saarbrücken, Germany — {theisel, hpseidel}@mpi-sb.mpg.de

Abstract

We present the first algorithm for constructing 3D vector fields based on their topological skeleton. The skeleton itself is modeled by interactively moving a number of control polygons. Then a piecewise linear vector field is automatically constructed which has the same topological skeleton as modeled before. This approach is based on a complete segmentation of the areas around critical points into sectors of different flow behavior. Based on this, we present the first approach to visualizing higher order critical points of 3D vector fields.

Categories and Subject Descriptors (according to ACM CCS): I.3.3 [Computer Graphics]: Line and Curve Generation I.3.7 [Computer Graphics]: Three-Dimensional Graphics and Realism

1. Introduction

Vector fields play an important role in many processes and phenomena of science and engineering. Hence the visualization of vector fields has become one of the most important subfields of Scientific Visualization. A variety of techniques have been developed to compute expressive visual representations of 2D and 3D vector fields. Among them, topological methods have gained a rather high popularity because they give the opportunity to represent even complex vector field structures in terms of only a small number of graphical primitives. After their introduction as a visualization tool in [HH89], a number of extensions have been proposed ([SKMR98, TKH00, dLvL99a, WS01, TWHS03]). Topological methods are used to simplify [dLvL99a, dLvL99b, TSH00, TSH01], smooth [WJE01], and compress [LRR00, TRS03] vector fields.

While most of the vector fields to be visualized are obtained by simulation or measurement processes, [The02] presents an approach to modeling 2D vector fields of higher order topology, i.e. consisting of higher order critical points. This approach is based on two steps. First, the topological skeleton is interactively modeled by defining critical points and separation curves. Then a piecewise linear vector field is constructed which has the topological skeleton modeled before. The approach is also applied for a topology based compression technique. Unfortunately, the methods in [The02] are strictly limited to 2D vector fields because of the following reasons:

- [The02] uses a complete segmentation of the areas around a 2D critical point into sectors of different flow behavior. Such a segmentation of 3D critical points does not exist yet in the Visualization and Computer Graphics community. In fact, only first order critical points and the index of higher order critical points ([MR02]) have been considered up to now.
- Contrary to the 2D case, separatrices of 3D vector fields are particular stream surfaces. They tend to have a complex behavior even for rather simple vector fields ([TWHS03]), making it a cumbersome (or even impossible) task to model them for instance as a parametric surface.
- There exists no approach to create a vector field which has a stream surface coinciding with a modeled parametric surface.

It is the purpose of this paper to present the (to the best of our knowledge) first approach to modeling 3D vector fields of arbitrary topology. We extend the main ideas of [The02] to 3D and give solutions for the three problems mentioned above. In particular, we introduce a complete classification of 3D critical points into an arbitrary number of sectors of different flow behavior. Based on this we present the first approach to visualizing higher order 3D critical points by ap-

propriate icons. To overcome the second and third problem, we adapt the recently introduced concept of saddle connectors ([TWHS03]) by modeling not the separation surfaces themselves but only their intersection curves. The resulting algorithm is a two-step approach. First the user models a 3D topological skeleton, then a vector field is automatically constructed from this. From the users's point of view, the problem of modeling a vector field is reduced to the problem of modeling a topological skeleton by a number of control polygons.

The rest of the paper is organized as follows: section 2 gives some motivation to create 3D vector fields by a modeling approach. Section 3 collects the most important concepts of 3D vector field topology and introduces a segmentation of the areas around a critical point into sectors of different flow behavior. Section 4 introduces an approach to model and visualize the topological skeleton of a 3D vector field. Section 5 shows how to construct a vector field from a modeled skeleton. Section 6 demonstrates applications and examples while conclusions are drawn in section 7.

2. Why Modeling Vector Fields?

The common workflow in Scientific Visualization starts with an unknown data set, which mostly resulted from a simulation or an experiment. This data gets analyzed, visualized and interpreted to yield a higher understanding of the processes inherent to it. As an example, for the topological treatment of vector fields one would extract the topology from the data set and display it.

So why should one do the opposite by modeling a topological skeleton and constructing a vector field out of this? The authors believe that this approach can be applied in a number of situations.

Pattern Matching: One way of detecting features in vector fields is to create a reference vector field consisting of the desired feature, and compute its local similarity to the real data set [ES03, HEWK03]. The modeling approach may help to construct more involved patterns and therefore allow to search for more involved features in the data set.

Topology preserving compression: In most cases, the memory requirements for storing a topological skeleton are much smaller than for the vector field itself ([The02]). This can be used for compression by just saving the topology and reconstructing a new vector field out of this later on. The construction methods presented in this paper guarantee that all topological features of the original data set are contained in the compressed one as well.

Topological simplification: Vector fields from numerical simulations may contain a very high number of critical points making a topological visualization difficult to interpret. The simplification method described in [TSH00] tackles this problem by merging adjacent critical points to one higher order critical point in 2D. The algorithms presented in this paper, especially the treatment of higher order critical points, form the basis of topological simplification methods for 3D vector fields.

Optimizing flow: The flow around an airfoil is subject to large efforts in order to increase the desired lift and to reduce the parasitic drag. These performance enhancements are achieved by changing the geometry (aerodynamic design) of the airfoil and controlling separation using air injection. Successful flow control strategies have mostly been based on a good physical understanding, which is more often achieved by a qualitative analysis as opposed to a quantitative one. Topology can aid this physical understanding not only by its visualization, but also by the ability to manipulate the original topology and to reconstruct the flow field out of this. This leads to a susceptibility study elucidating beneficial and detrimental changes to lift, drag and other parameters, because one can compute these measures for the reconstructed flow and compare it with the original ones. Thus, the beneficial topological structures for lift and drag can be identified. As a part of reverse engineering, actuation and sensing solutions for these beneficial structures can be developed. This computationally efficient topology-aided sensitivity analysis can guide heavy-duty numerical simulations and experimental setups.

Education and Testing: For the educational explanation of topological and other visualization methods, the algorithms described in this paper can be used to create simple and illustrative data sets. Modeled vector fields may also serve as test data while developing new visualization techniques, but for their evaluation real data sets have to be used.

It is beyond the scope of this paper to present solutions for all the applications mentioned above. Some of them may even lead to new research directions once a modeling approach is available.

3. The Topology of 3D Vector Fields

The idea of vector field topology is to separate regions of different flow behavior in the field. The main components of a topological skeleton are critical points and separation surfaces. We treat them in the next two subsections. In addition, there are other topological features (boundary switch curves [MBHJ03, WTHS04] or closed stream lines [WS01]) which are not considered in this paper.

3.1. Critical Points

It is a well-known fact ([FG82]) that for 2D vector fields a critical point can be described by detecting regions of different flow behavior around it. These regions are separated by particular stream lines called separatrices. There exist three kinds of regions (Figure 1):

- **Parabolic sectors:** all stream lines *either* start *or* end in the critical point.

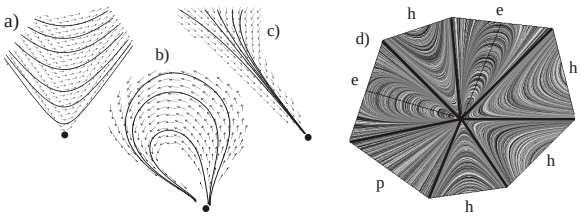

Figure 1: *Sectors of a 2D critical point. a) hyperbolic sector, b) elliptic sector, c) parabolic sector; d) example of a critical point consisting of 4 hyperbolic, 2 elliptic and one parabolic sector (from [The02]).*

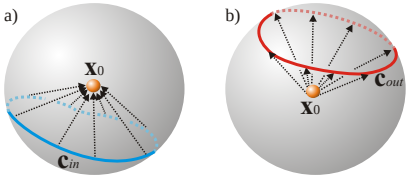

Figure 2: *The sphere model. a) describing an inflow surface at $\mathbf{x}_0$ by a closed curve $\mathbf{c}_{in}$ on $\mathbf{s}$: integrating $\mathbf{c}_{in}$ in forward direction ends in $\mathbf{x}_0$; b) outflow surface described by a closed curve $\mathbf{c}_{out}$ on $\mathbf{s}$.*

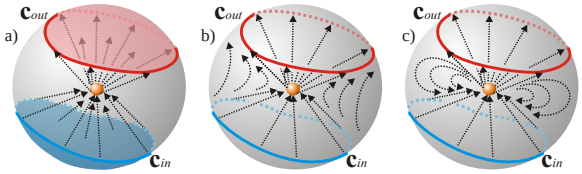

Figure 3: *Sectors of a 3D critical point. a) outflow sector (red area) inside $\mathbf{c}_{out}$, and inflow sector (blue area) inside $\mathbf{c}_{in}$; b) hyperbolic sector between $\mathbf{c}_{in}$ and $\mathbf{c}_{out}$; c) elliptic sector between $\mathbf{c}_{in}$ and $\mathbf{c}_{out}$.*

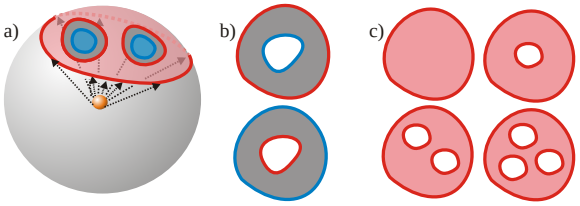

Figure 4: *a) an outflow sector is further divided into two hyperbolic sectors (gray) and two inflow sectors (blue); b) hyperbolic and elliptic sectors are topologically equivalent to a punctured disk; c) parabolic sectors are topologically equivalent to a disk with an arbitrary number of holes.*

- **Elliptic sectors:** all stream lines start *and* end in the point.
- **Hyperbolic sectors:** all stream lines pass by the critical point except for the separatrices themselves.

Given a 3D vector field $\mathbf{v} : \mathbb{R}^3 \rightarrow \mathbb{R}^3$, a point $\mathbf{x}_0$ is a critical point if $\mathbf{v}(\mathbf{x}_0) = (0,0,0)^T$, and $\mathbf{v}(\mathbf{x}) \neq (0,0,0)^T$ for any other point in a certain neighborhood of $\mathbf{x}_0$. Although there exist profound mathematical studies of the behavior of higher order critical points in 3D ([Tak74, BD86, DI98]), up to now the Visualization and Computer Graphics community only considered the index of such a critical point ([MR02]). In the following we introduce a partition approach for 3D critical points.

A 3D critical point can be classified into sectors of different flow behavior. As in the 2D case, there are parabolic, elliptic and hyperbolic sectors which are separated by separation surfaces. Consider a small sphere $\mathbf{s}$ around a 3D critical point $\mathbf{x}_0$: We describe the different sectors of $\mathbf{x}_0$ as certain regions on $\mathbf{s}$. This way an *inflow surface* of $\mathbf{x}_0$ can be described by a closed curve $\mathbf{c}_{in}$ on $\mathbf{s}$ with the property that a stream line starting from any point of $\mathbf{c}_{in}$ ends in $\mathbf{x}_0$ by forward integration. Similarly, an *outflow surface* is described by a closed curve $\mathbf{c}_{out}$ with stream lines ending in $\mathbf{x}_0$ by backward integration. Figure 2 illustrates inflow and outflow surfaces of a critical point. Note that they may collapse to a line: this happens when $\mathbf{c}_{in}$ or $\mathbf{c}_{out}$ collapse to a point.

Consider one inflow and one outflow surface of $\mathbf{x}_0$ defined by $\mathbf{c}_{in}$ and $\mathbf{c}_{out}$ on $\mathbf{s}$. Keeping in mind that $\mathbf{s}$ covers a very small neighborhood of $\mathbf{x}_0$, $\mathbf{c}_{in}$ and $\mathbf{c}_{out}$ must not intersect. They divide $\mathbf{s}$ into three different regions: the region inside $\mathbf{c}_{in}$, the region inside $\mathbf{c}_{out}$, and the region between them (Figure 3). The region inside $\mathbf{c}_{in}$ is an *inflow sector*: all stream lines starting there end in $\mathbf{x}_0$ by forward integration. Similarly, the region inside $\mathbf{c}_{out}$ is an *outflow sector*. As in the 2D case, both inflow and outflow sectors are *parabolic sectors*. The region between $\mathbf{c}_{in}$ and $\mathbf{c}_{out}$ may be either a *hyperbolic sector* or an *elliptic sector*. In case of a hyperbolic sector, all stream lines pass by $\mathbf{x}_0$, for an elliptic sector all stream line start and end in $\mathbf{x}_0$. Figure 3 illustrates the different sectors.

After showing how $\mathbf{s}$ is segmented by one inflow and one outflow curve, we consider the presence of additional inflow/outflow curves. Doing so, each of the sectors can be further subdivided into more sectors. Figure 4a shows an example where an outflow sector is divided into two hyperbolic and two inflow sectors. This example also shows a property about the shape of the different sectors: each hyperbolic and each elliptic sector have a strip shaped topology, i.e. they are topologically equivalent to a punctured disk (Figure 4b). On the contrary, parabolic sectors are topologically equivalent to a disk with an arbitrary number of holes (or they cover the whole sphere) (Figure 4c).

Given this classification of critical points, the well-known first-order critical points fit into this system as well. They have a non-vanishing Jacobian and are therefore governed by the first-order partials. We can distinguish sources, sinks and saddles. Sources and sinks consist of one parabolic sector covering the whole surface of $\mathbf{s}$. A saddle consists of an out-

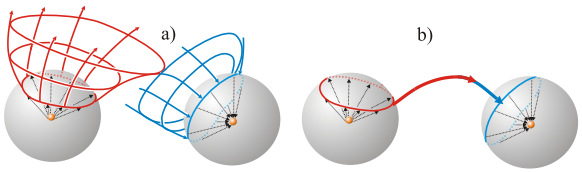

Figure 5: *a) the outflow surface of one critical point intersects the inflow surface of another one; b) the intersection curve is a stream line, called connector.*

flow plane and two degenerate inflow surfaces (or the other way around, an inflow plane and two degenerate outflow surfaces). Hence, a saddle consists of two hyperbolic sectors.

In addition to our segmentation of a 3D critical point there are other topological features which we do not treat here. For example, consider a 2D critical point with imaginary eigenvalues of the Jacobian producing spiral-shaped stream lines around the point. Such stream lines may also occur in an inflow/outflow surface of a 3D critical point, which we did not include into the classification here.

3.2. Separatrices

For 3D vector fields, separatrices are certain stream surfaces separating areas of different flow behavior. The inflow/outflow surfaces of a critical point have exactly this behavior. Thus, separation surfaces can be obtained by a stream surface integration starting from a critical point into the direction of an inflow/outflow surface. Unfortunately, stream surfaces tend to have a rather complicated behavior making their visualization cluttered and hard to interpret ([TWHS03]). Moreover, modeling these surfaces is a cumbersome task. [TWHS03] presents a solution for separation surfaces emanating from first order saddle points: instead of the surfaces themselves, only their intersection curves (*saddle connectors*) are extracted and visualized. For our modeling approach we adapt this idea by modeling not the separation surfaces but only their intersection curves. They are certain stream lines starting in the inflow surface of a critical point and ending in the outflow surface of another (or the same) critical point. We call them *connectors*. Figure 5 gives an illustration. Using them for modeling the topological skeleton gives a certain control over the behavior of the separation surfaces, though it is not a full replacement.

4. Modeling and Visualizing the Topological Skeleton

After introducing the topological skeleton, we now describe how to interactively model it. Based on this, we introduce the first icon based visualization technique for higher order critical points.

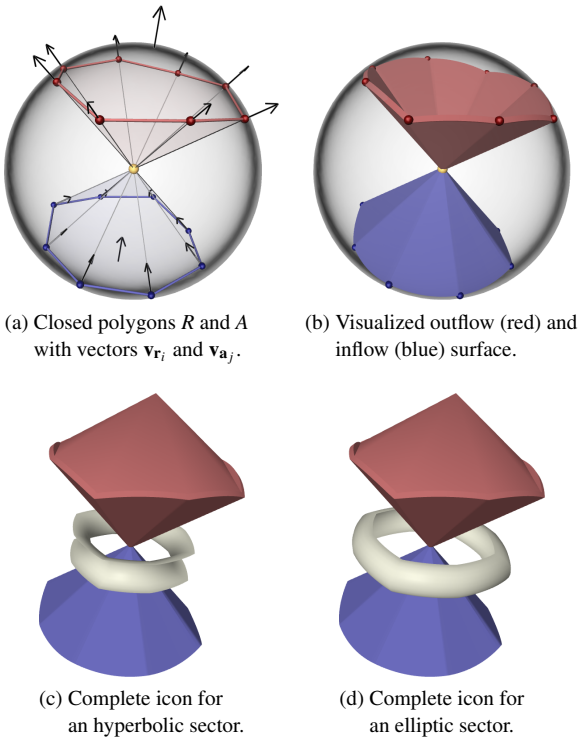

(a) Closed polygons R and A with vectors $\mathbf{v}_{\mathbf{r}_i}$ and $\mathbf{v}_{\mathbf{a}_j}$.

(b) Visualized outflow (red) and inflow (blue) surface.

(c) Complete icon for an hyperbolic sector.

(d) Complete icon for an elliptic sector.

Figure 6: *Modeling a critical point and its visualization.*

4.1. Critical Points

To model a critical point $\mathbf{x}_0$, we use the sphere model (Figure 2) introduced in section 3: we place a number of control points $\mathbf{r}_i$ and $\mathbf{a}_j$ on the sphere $\mathbf{s}$ around $\mathbf{x}_0$ and provide them with vectors $\mathbf{v}_{\mathbf{r}_i}$ and $\mathbf{v}_{\mathbf{a}_j}$. These vectors describe the behavior of $\mathbf{v}$ around $\mathbf{x}_0$. In particular, an outflow surface is represented by a closed polygon $R = (\mathbf{r}_0, \ldots, \mathbf{r}_n)$ on $\mathbf{s}$ with the supplied vectors $\mathbf{v}_{\mathbf{r}_i} = \lambda_{\mathbf{r}_i}(\mathbf{r}_i - \mathbf{x}_0)$ for positive $\lambda_{\mathbf{r}_i}$. This way, only the length $\lambda_{\mathbf{r}_i}$ of the vectors $\mathbf{v}_{\mathbf{r}_i}$ can be chosen by the user. An inflow surface is modeled in a similar way as a closed polygon $A = (\mathbf{a}_0, \ldots, \mathbf{a}_m)$ with $\mathbf{v}_{\mathbf{a}_j} = \lambda_{\mathbf{a}_j}(\mathbf{x}_0 - \mathbf{a}_j)$ and $\lambda_{\mathbf{a}_j} > 0$. Figure 6a shows an example. Note that the closed polygons R and A correspond to the closed curves $\mathbf{c}_{out}$ and $\mathbf{c}_{in}$ introduced in section 3.

Once all inflow and outflow surfaces are modeled, all regions between an inflow and an outflow surface have to be marked either as a hyperbolic or elliptic sector. The remaining areas are parabolic sectors and do not have to be specified.

In order to visualize a critical point, we place an appropriate icon into its location. For this icon, we first visualize the outflow surfaces in a red color and the inflow surfaces in a blue color: for an outflow surface described by the closed polygon $R = \mathbf{r}_0, \ldots, \mathbf{r}_n$, we represent it by the red triangles $(\mathbf{x}_0, \mathbf{r}_i, \mathbf{r}_{(i+1) mod\ n})$, where the edge $(\mathbf{r}_i, \mathbf{r}_{(i+1) mod\ n})$ is dis-

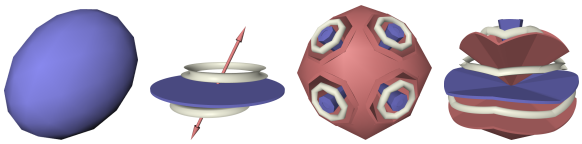

(a) $n_h = 0$, $n_e = 0$. (b) $n_h = 2$, $n_e = 0$. (c) $n_h = 0$, $n_e = 4$. (d) $n_h = 1$, $n_e = 2$.

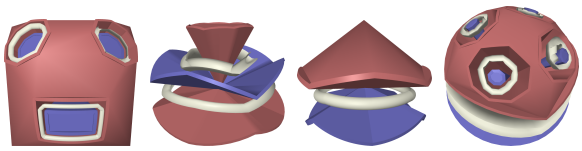

(e) $n_h = 1$, $n_e = 2$. (f) $n_h = 1$, $n_e = 1$. (g) $n_h = 0$, $n_e = 1$. (h) $n_h = 5$, $n_e = 1$.

Figure 7: *8 critical points with varying numbers n_h and n_e of hyperbolic and elliptic sectors.*

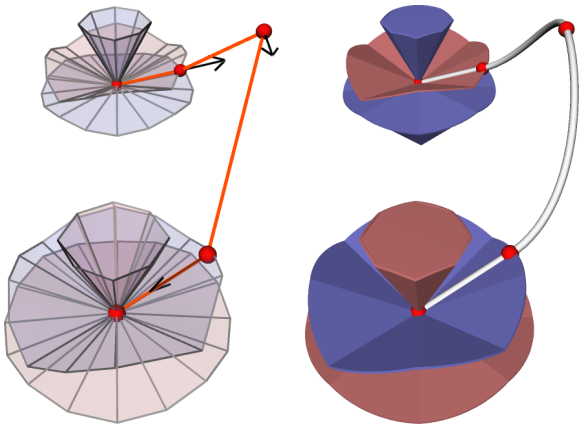

(a) Control polygon. (b) Visualization.

Figure 8: *Modeled connector with one intermediate point.*

torted proportional to $\lambda_{\mathbf{r}_i}$ and $\lambda_{\mathbf{r}_{(i+1) mod\ n}}$. In a similar way, inflow surfaces are represented by a number of blue triangles. Figure 6b shows an example. Note that we added some "thickness" to the surfaces to enhance the visualization. If an inflow/outflow surface degenerates to a line, we use a blue or red 3D arrow to represent its inflow/outflow direction at $\mathbf{x}_0$. Figure 7b shows an example of this.

The last step to create the icon is to represent the different sectors. For hyperbolic and elliptic sectors we place a surface strip around $\mathbf{x}_0$ which shape gives the distinction between the two sectors. In fact, the shape of the strips is a representation of the different flow behavior in the sectors. Figure 6c shows the icon for a hyperbolic sector, while figure 6d shows an elliptic sector. The remaining parabolic sectors are simply represented by filling the areas with a surface. We used a piecewise linear surface consisting of the vertices of R_i or A_j. Figure 7 shows a collection of 8 critical points where the number of hyperbolic and elliptic sectors varies between 0 and 5.

4.2. Connectors and Stream Lines

In order to model the connectors of a 3D vector field, we first have to define their start and end points. The start point is specified by a critical point $\mathbf{x}_0$, an outflow surface described by the closed polygon $R = (\mathbf{r}_0, ..., \mathbf{r}_n)$, and a point on this polygon. Similarly, the end point of a connector is defined by a point on an inflow surface. In addition, we allow a number of intermediate points which are supplied with vectors; the connector is supposed to interpolate them both in location and tangent direction. Figure 8a shows a connector between two critical points which is defined by starting point, end point, and one intermediate point. To visualize a connector, we assume a piecewise C^1 continuous cubic curve interpolating all points both in location and tangent direction (Figure 8b).

A vector field may have areas where only a few (or even no) topological features are present. For these areas the modeling of the topological skeleton does not give any information to build the vector field. To deal with such areas, we additionally allow the user to place arbitrary stream lines into the domain. They are modeled - similar to the connectors - as a sequence of points supplied with a vector information. Then the stream lines are the interpolating (both in location and tangent) piecewise C^1 continuous cubic curves. These stream lines are later incorporated into the construction of the vector field, even though they are not part of the topological skeleton.

5. Construction of the Vector Field

Once the topological skeleton is modeled, we have to construct a vector field which has the specified skeleton. We use a piecewise linear vector field, i.e. we construct a tetrahedrization of the domain where each of its vertices is supplied with a vector. The construction is done in a fully-automatic way.

5.1. Critical Points

To construct the tetrahedrization around a critical point $\mathbf{x}_0$, we extend the approach of [TSH00] and [The02] to 3D: a vertex with a zero vector is placed at $\mathbf{x}_0$, around this a number of tetrahedra sharing $\mathbf{x}_0$ as a vertex are placed. For these tetrahedra, we essentially use the vertices of the polygons defining inflow and outflow surfaces. We give the following **algorithm** to tetrahedrize the region around a critical point:

1. Consider a sphere $\mathbf{s}$ around $\mathbf{x}_0$ such that $\mathbf{s}$ does not intersect any sphere around another critical point. We assume that k outflow surfaces are present which are described by the k closed polygons $R_0 = (\mathbf{r}_{0,0}, ..., \mathbf{r}_{n_0,0}), ..., R_{k-1} = (\mathbf{r}_{0,k-1}, ..., \mathbf{r}_{n_{k-1},k-1})$. We further assume that ℓ inflow

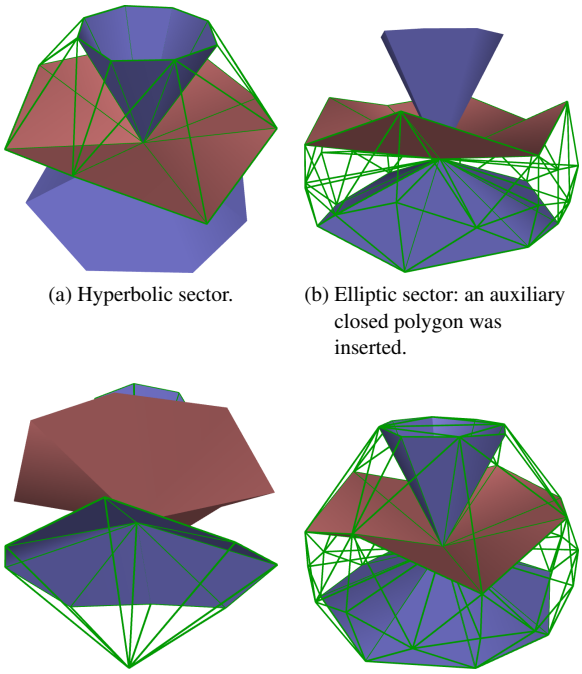

(a) Hyperbolic sector. (b) Elliptic sector: an auxiliary closed polygon was inserted.

(c) Both parabolic sectors. (d) Complete tetrahedrization.

Figure 9: *Tetrahedrization of different sectors of a critical point.*

surfaces are described by the closed polygons $A_0 = (\mathbf{a}_{0,0},...,\mathbf{a}_{m_0,0}),...,A_{\ell-1} = (\mathbf{a}_{0,\ell-1},...,\mathbf{a}_{m_{\ell-1},\ell-1})$.

2. Insert all start and end points of connectors into the closed polygons. If a connector starts at $\mathbf{x}_0$ in the i-th outflow surface, its starting point has to be inserted as a new vertex into R_i. Similarly, if a connector ends in $\mathbf{x}_0$ in the j-th inflow surface, its end point is inserted into A_j (cf. Figure 8a). This is necessary to get consistent tetrahedrizations of critical points and connectors later on.
3. Tetrahedrize all hyperbolic sectors. If the modeler gives a hyperbolic sector between the i-th outflow surface and the j-th inflow surface, we triangulate the strip between R_i and A_j by using a constrained Delaunay triangulation. The obtained triangles are converted to tetrahedra by connecting them with $\mathbf{x}_0$ (Figure 9a).
4. Tetrahedrize all elliptic sectors. If there is an elliptic sector between the i-th outflow surface and the j-th inflow surface, we have to construct an auxiliary closed polygon $H_{i,j} = (\mathbf{h}_{0,i,j},...,\mathbf{h}_{n_{i,j},i,j})$ between R_i and A_j. To do so, we imagine a constrained Delaunay triangulation between R_i and A_j. If the edge $(\mathbf{r}_{e,i},\mathbf{a}_{f,j})$ is part of this triangulation, we insert the point $(\mathbf{r}_{e,i}+\mathbf{a}_{f,j})/2$ into $H_{i,j}$ and provide it with the vector $\mathbf{a}_{f,j}-\mathbf{r}_{e,i}$. Then we apply a constrained Delaunay triangulation between R_i and $H_{i,j}$, and another one between $H_{i,j}$ and A_j. The obtained triangles are tetrahedrized by connecting them with $\mathbf{x}_0$ (Figure 9b).

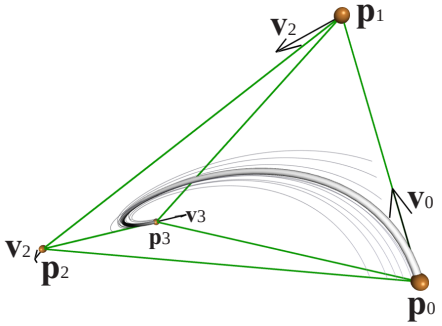

Figure 10: *Setup of theorem 1: one of the stream lines of the linear vector field coincides with the cubic Bézier curve.*

5. Tetrahedrize all parabolic sectors. All remaining areas on $\mathbf{s}$ are triangulated by a constrained Delaunay triangulation. If necessary, additional inflow/outflow points on $\mathbf{s}$ have to be inserted. The triangles are tetrahedrized by connecting them with $\mathbf{x}_0$ (Figure 9c).

5.2. Connectors and Stream Lines

To tetrahedrize connectors and stream lines, we keep in mind that we modeled them as piecewise cubic curves. The stream lines of a linear vector field are certain exponential curves which can be expressed in a closed form ([Nie97]). Fortunately it turns out that the class of non-planar cubic curves is contained in the class of stream lines of linear vector fields. We give the following

Theorem 1 Given are 4 non-coplanar points $\mathbf{p}_0,...,\mathbf{p}_3$ which are equipped with the 3D vectors $\mathbf{v}_0,...,\mathbf{v}_3$. This way a linear vector field $\mathbf{v}$ is defined inside the tetrahedron $\mathbf{p}_0,...,\mathbf{p}_3$. If $\mathbf{v}_0,...,\mathbf{v}_3$ are chosen as

$$\mathbf{v}_0 = \lambda_0(\mathbf{p}_1-\mathbf{p}_0) \quad , \quad \mathbf{v}_3 = \lambda_3(\mathbf{p}_3-\mathbf{p}_2) \tag{1}$$

$$\mathbf{v}_1 = \frac{1}{3}\lambda_3(\mathbf{p}_1-\mathbf{p}_0) + \frac{2}{3}\lambda_0(\mathbf{p}_2-\mathbf{p}_1) \tag{2}$$

$$\mathbf{v}_2 = \frac{2}{3}\lambda_3(\mathbf{p}_2-\mathbf{p}_1) + \frac{1}{3}\lambda_0(\mathbf{p}_3-\mathbf{p}_2) \tag{3}$$

for certain $\lambda_0,\lambda_3 > 0$, then the following property holds: the stream line of $\mathbf{v}$ starting in $\mathbf{p}_0$ is identical to the cubic Bézier curve defined by the Bézier points $\mathbf{p}_0,...,\mathbf{p}_3$.

Figure 10 illustrates the setup of theorem 1. To prove this theorem, we consider the Bézier curve $\mathbf{x}(t) = \sum_{i=0}^{3} B_i^3(t)\,\mathbf{p}_i$ where $B_i^3(t)$ are the cubic Bernstein polynomials. We have to show that $\dot{\mathbf{x}}(t) \times \mathbf{v}(\mathbf{x}(t)) = (0,0,0)^T$ for any t. Inserting (1)-(3) into this equation, this is a straightforward exercise in algebra. Note that the vector field generated by (1)-(3) generally has only one cubic curve as a stream line: the stream lines around $\mathbf{x}(t)$ are generally no polynomial curves.

Theorem 1 does not only show that non-planar cubic curves are contained in piecewise linear vector fields, it

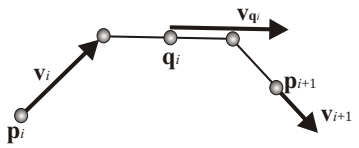

(a) Dividing an almost planar cubic part into two quadratic parts.

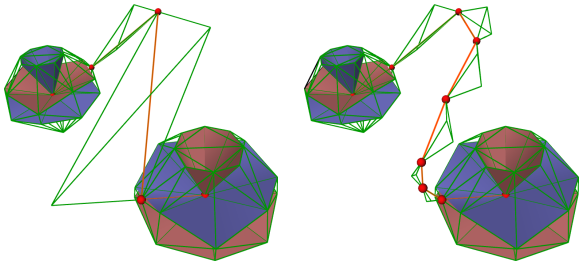

(b) Intersecting tetrahedra.

(c) After repeated subdivision of intersecting tetrahedra.

Figure 11: *Subdivision of a connector or stream line.*

also shows how to construct this vector field. Given a cubic curve by its Bézier polygon $\mathbf{p}_0,\ldots,\mathbf{p}_3$, we add the tetrahedron $\mathbf{p}_0,\ldots,\mathbf{p}_3$ with the vectors $\mathbf{v}_0,\ldots,\mathbf{v}_3$ obtained from (1)-(3) to the tetrahedrization. Unfortunately, this approach is not applicable if $\mathbf{p}_0,\ldots,\mathbf{p}_3$ are nearly coplanar, which leads to a degenerate tetrahedron. (In fact, planar cubics are *not* contained in the class of stream lines of linear vector fields.) In this case we subdivide the cubic curve into two quadratic pieces (Figure 11a): if the cubic between the points-with-vectors $(\mathbf{p}_i,\mathbf{v}_i)$ and $(\mathbf{p}_{i+1},\mathbf{v}_{i+1})$ is nearly planar, we insert a new point-with-vector $(\mathbf{q}_i,\mathbf{v}_{\mathbf{q}_i})$ with $\mathbf{q}_i = (\mathbf{p}_i+\mathbf{v}_i+\mathbf{p}_{i+1}-\mathbf{v}_{i+1})/2$ and $\mathbf{v}_{\mathbf{q}_i} = (\mathbf{p}_{i+1}-\mathbf{v}_{i+1})-(\mathbf{p}_i+\mathbf{v}_i)$. Then $(\mathbf{p}_i,\mathbf{v}_i)$ and $(\mathbf{q}_i,\mathbf{v}_{\mathbf{q}_i})$ are coplanar, as well as $(\mathbf{q}_i,\mathbf{v}_{\mathbf{q}_i})$ and $(\mathbf{p}_{i+1},\mathbf{v}_{i+1})$. We then construct a piecewise linear vector field yielding the parabola between these points as described in ([The02]).

Once we have constructed one (or two) tetrahedra for each cubic segment of each connector and stream line, these tetrahedra might intersect each other as well as other tetrahedra coming from critical points. In this case, they have to be subdivided into two new tetrahedra by subdividing the underlying cubic or quadratic Bézier curve. This process is repeated until no tetrahedra intersect any more (Figure 11b–c).

After tetrahedrizing all critical points and connectors (i.e. the topological skeleton), we have to fill the remaining areas of the domain which are not tetrahedrized yet. To do so, we define a bounding box around the domain and apply a constrained Delaunay tetrahedrization incorporating the 8 vertices of the bounding box. For this task, we used an adaption of the freely available library TetGen [Si02]. This way a number of new vertices may be created. To assign them with vectors (as well as to assign the vertices of the bounding box with vectors), we compute a weighted average of the vectors of all vertices sharing an edge with the new vertex; the weights are the inverse of the distance of the vertices.

5.3. Topological Completeness and Consistency

Our vector field construction approach described above guarantees that all topological features (critical points and connectors) of the skeleton are contained in the vector field. However, we can *not* guarantee that no additional critical points and connectors appear.

The appearance of additional connectors is due to the fact, that our modeling approach does not allow full control over the behavior of the separation surfaces. To achieve this one would need to model them as e.g. parametric surfaces, which is a cumbersome or even impossible task. Furthermore, there seems to be no approach to create a vector field with stream surfaces coinciding to such parametric surfaces. However, depending on the scenario one can try to model stream lines in order to give the field (and its stream surfaces) a certain direction in a specific area (cf. Figure 14b).

There are two main reasons for the appearance of additional critical points. First, the indices of the modeled critical points may sum up to a high (positive or negative) number. This happens if e.g. only sources have been modeled, but no sinks or saddles. As vector fields usually tend to have an index close to zero, additional critical points are likely to appear in this case. Second, additional critical points may be due to an inappropriate tetrahedrization of the remaining areas or an inappropriate choice of the vectors at the vertices of the bounding box. A more involved strategy may make them disappear. However, such an optimized tetrahedrization or choice of vectors is beyond the scope of this paper.

6. Examples

In this section we demonstrate our approach to model a number of 3D vector fields of different topological behavior.

Figure 12a shows a modeled topological skeleton consisting of 6 critical points and 8 connectors. Each of the critical points consists of two hyperbolic sectors and is actually a first order saddle point. Each of the connectors was defined by specifying start and end point and omitting any intermediate points. Thus, each connector consists of one cubic segment. Figure 12b shows the result of the tetrahedrization of the critical points and the connectors. In this figure we can clearly see that each connector is constructed in one tetrahedron. Figure 12c shows the complete tetrahedrization of the piecewise linear vector field consisting of 256 tetrahedra. Figures 12d and 12e show different visualizations of the newly constructed vector field. Figure 12d shows a stream surface integration of the separation surfaces. They are color coded in red (outflow surface) and blue (inflow surface). Figure 12e shows the extraction of saddle connectors [TWHS03] revealing that they coincide with the mod-

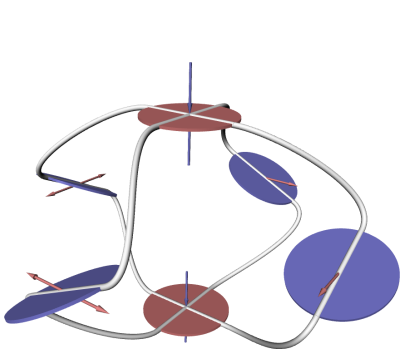

(a) Modeled topological skeleton.

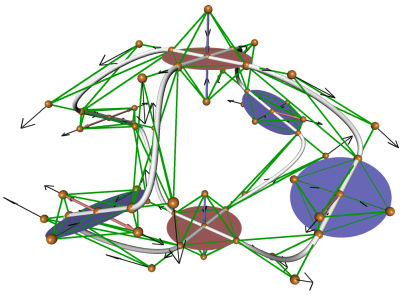

(b) Tetrahedrization of critical points and connectors.

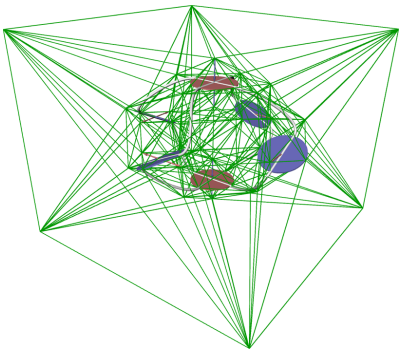

(c) Complete tetrahedrization.

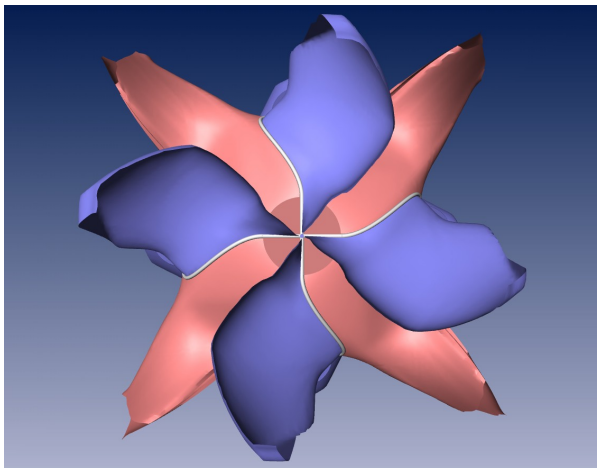

(d) Separation surfaces of constructed vector field. View from top.

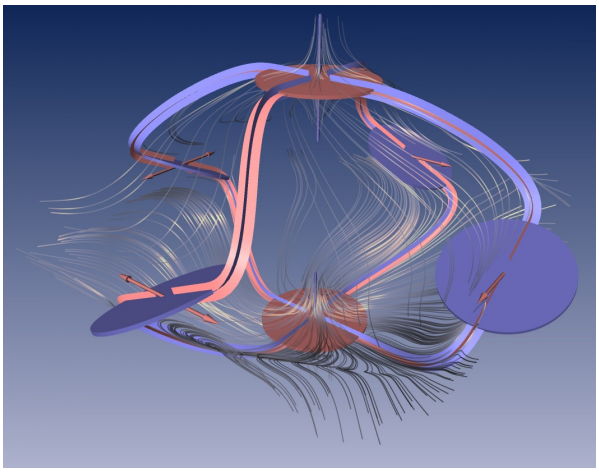

(e) Saddle connectors and stream lines of constructed vector field.

Figure 12: *Example 1.*

eled connectors of figure 12a. In addition, figure 12e shows a number of illuminated stream lines [ZSH96].

Figure 13 shows another modeled topological skeleton. We included this example to demonstrate that our approach can also handle a higher number of connectors between two critical points. In this example, we alternately connected the outflow surface of the critical point in the middle with the inflow surfaces of the two other critical points. All the connectors are modeled without intermediate points. Figure 13a illustrates the tetrahedrization of the skeleton, showing that each of the connectors is represented by 4 quadratic pieces. The automatic subdivision (which is responsible for this) first subdivided the modeled planar cubic curves into two quadratic curves, then each of them was subdivided one more time to remove the intersections of the defining tetrahedra of adjacent connectors. Figure 13b shows the integrated separation surfaces in a semi-transparent way. Note how the red separation surface follows all connectors to the other two critical points. This example exemplifies that the control of separation surfaces using connectors is possible to a certain degree.

In figure 14 we modeled a vector field consisting of 80 critical points, 80 connectors, and 14 additional stream lines. It describes a laminar flow in which 20 regions of different flow behavior are inserted. Each of these regions consists of a source and a sink and is bounded by the separation surfaces of two critical points with two hyperbolic sectors (Figure 14a). We modeled 4 connectors between each of these critical points. The regular setup of this example ensures that the two separation surfaces coincide. Inside the areas of these surfaces we have a simple behavior: every stream line starts in the source and ends in the sink. Outside these areas we modeled a turbulence-free flow around it, which is laminar in a certain distance from the inserted regions. To do so, we included a number of straight stream lines into the flow. Figure 14c shows a visualization of the resulting piecewise linear vector field consisting of 8198 tetrahedra: two inserted LIC planes reveal the laminar flow in a distance of

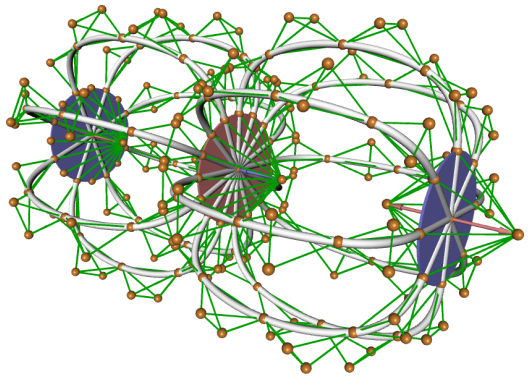

(a) Tetrahedrization of the modeled skeleton.

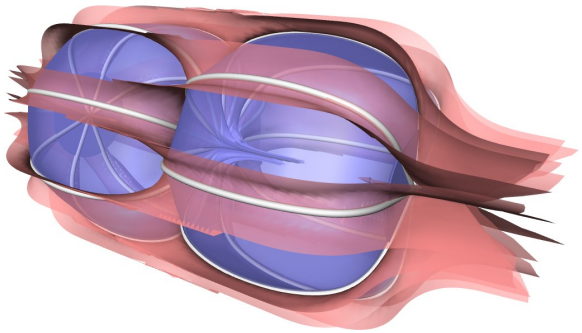

(b) Separation surfaces and modeled connectors.

Figure 13: *Example 2.*

the inserted areas as well as the flow behavior inside it. In addition, a number of illuminated stream lines are inserted.

7. Conclusions

In this paper we made the following contributions:

- We introduced a classification of 3D higher order critical points to the Computer Graphics and Visualization community.
- We introduced the first visualization technique for higher order critical points.
- We showed how to model a topological skeleton as a collection of control polygons.
- We showed that non-planar cubic polynomial curves are contained in the class of stream lines of linear 3D vector fields.
- We introduced an approach to automatically construct a piecewise linear vector field from the previously modeled topological skeleton.

We see the research reported in this paper as a starting point for a number of ongoing research projects which are mostly mentioned in section 2. In particular, for the next future we intend to apply the approach for pattern matching and topological simplification.

Acknowledgements

We thank Bernd R. Noack and Jan Sahner for the fruitful discussions. We thank Hang Si for his effort to develop Tetgen [Si02] and his insightful tips on how to use it for our purposes.

All visualizations in this paper have been created using AMIRA – a system for advanced 3D visualization and volume modeling [SHW04] (see `http://amira.zib.de/`).

References

[BD86] BONCKAERT P., DUMORTIER F.: Smooth invariant curves for germs of vector fields in $\mathbb{R}^3$ whose linear part generates rotations. *J. Diff. Eqns. 62* (1986), 95–116.

[DI98] DUMORTIER F., IBÁÑEZ S.: Singularities of vector fields on $\mathbb{R}^3$. *J. Nonlinearity. 11* (1998), 1037–1047.

[dLvL99a] DE LEEUW W., VAN LIERE R.: Collapsing flow topology using area metrics. In *Proc. IEEE Visualization '99* (1999), pp. 149–354.

[dLvL99b] DE LEEUW W., VAN LIERE R.: Visualization of global flow structures using multiple levels of topology. In *Data Visualization 1999. Proc. VisSym 99* (1999), pp. 45–52.

[ES03] EBLING J., SCHEUERMANN G.: Clifford convolution and pattern matching on vector fields. In *Proc. IEEE Visualization 2003* (2003), pp. 193–200.

[FG82] FIRBY P., GARDINER C.: *Surface Topology*. Ellis Horwood Ltd., 1982, ch. 7, pp. 115–135. Vector Fields on Surfaces.

[HEWK03] HEIBERG E., EBBERS T., WIGSTRÖM L., KARLSSON M.: Three dimensional flow characterization using vector pattern matching. *IEEE Transactions on Visualization and Computer Graphics 9*, 3 (2003), 313–319.

[HH89] HELMAN J., HESSELINK L.: Representation and display of vector field topology in fluid flow data sets. *IEEE Computer 22*, 8 (August 1989), 27–36.

[LRR00] LODHA S., RENTERIA J., ROSKIN K.: Topology preserving compression of 2D vector fields. In *Proc. IEEE Visualization 2000* (2000), pp. 343–350.

[MBHJ03] MAHROUS K., BENNETT J., HAMANN B., JOY K.: Improving topological segmentation of three-dimensional vector fields. In *Data Visualization 2003. Proc. VisSym 03* (2003), pp. 203–212.

[MR02] MANN S., ROCKWOOD A.: Computing singularities of 3D vector fields with geometric algebra. In *Proc. IEEE Visualization 2002* (2002), pp. 283–289.

[Nie97] NIELSON G.: Tools for computing tangent curves and topological graphs for visualizing piecewise linearly varying vector fields over triangulated domains. In *Scientific Visualization*, Nielson G., Hagen H.,, Müller H., (Eds.). IEEE Computer Society, 1997, pp. 527–562.

[SHW04] STALLING D., HEGE H.-C., WESTERHOFF M.: Amira – a highly interactive system for visual data analysis. In *Visualization Handbook* (2004), Johnson C. R., Hansen C. D., (Eds.), Academic Press.

[Si02] SI H.: Tetgen. a 3D delaunay tetrahedral mesh generator. v.1.2 users manual. *WIAS Technical Report*, 4 (2002). http://www.wias-berlin.de/publications/technicalreports/4/.

[SKMR98] SCHEUERMANN G., KRÜGER H., MENZEL M., ROCKWOOD A.: Visualizing non-linear vector field topology. *IEEE Transactions on Visualization and Computer Graphics 4*, 2 (1998), 109–116.

[Tak74] TAKENS F.: Singularities of vector fields. *Publ. Math. IHES 43* (1974), 47–100.

[The02] THEISEL H.: Designing 2D vector fields of arbitrary topology. *Computer Graphics Forum (Eurographics 2002) 21*, 3 (2002), 595–604.

[TKH00] TROTTS I., KENWRIGHT D., HAIMES R.: Critical points at infinity: a missing link in vector field topology. In *Proc. NSF/DoE Lake Tahoe Workshop on Hierarchical Approximation and Geometrical Methods for Scientific Visualization* (2000).

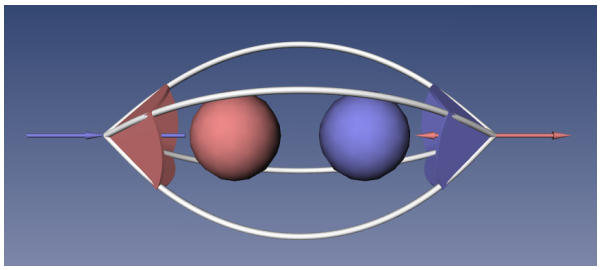

(a) Part of the skeleton that has been duplicated 20 times.

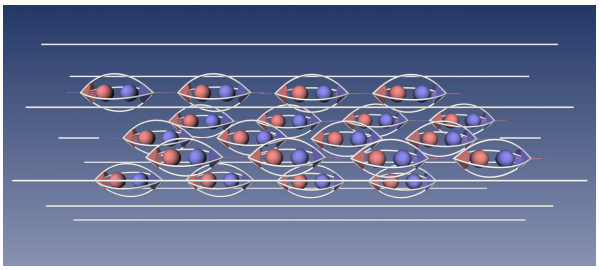

(b) Modeled skeleton with stream lines to laminarize the outer flow.

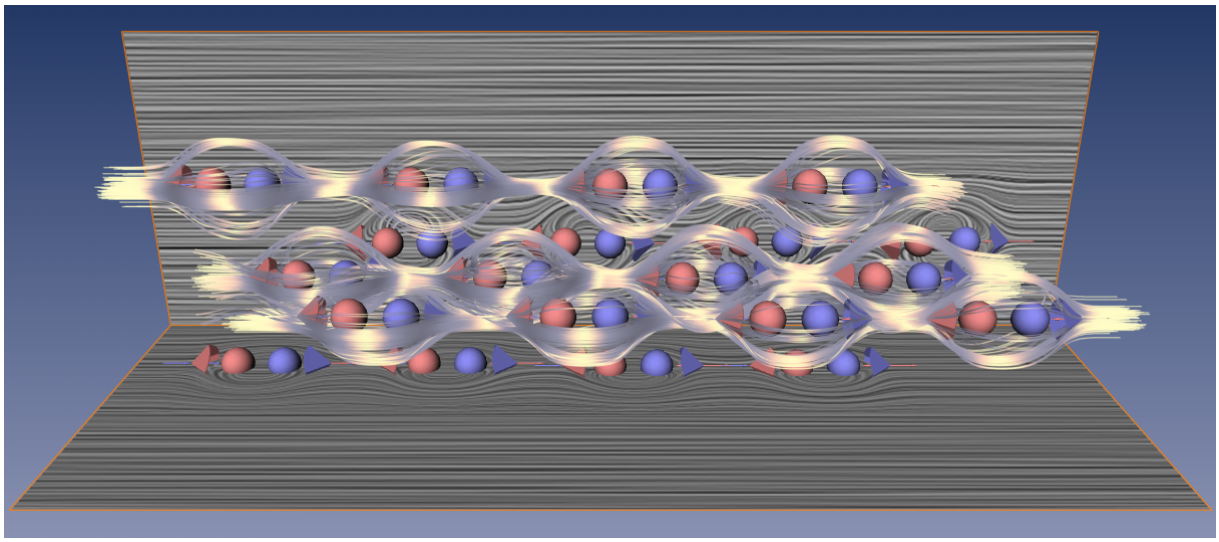

(c) Constructed vector field visualized using illuminated stream lines and LIC.

Figure 14: *Example 3.*

[TRS03] THEISEL H., RÖSSL C., SEIDEL H.-P.: Compression of 2D vector fields under guaranteed topology preservation. *Computer Graphics Forum (Eurographics 2003) 22*, 3 (2003), 333–342.

[TSH00] TRICOCHE X., SCHEUERMANN G., HAGEN H.: A topology simplification method for 2D vector fields. In *Proc. IEEE Visualization 2000* (2000), pp. 359–366.

[TSH01] TRICOCHE X., SCHEUERMANN G., HAGEN H.: Continuous topology simplification of planar vector fields. In *Proc. Visualization 01* (2001), pp. 159 – 166.

[TWHS03] THEISEL H., WEINKAUF T., HEGE H.-C., SEIDEL H.-P.: Saddle connectors - an approach to visualizing the topological skeleton of complex 3D vector fields. In *Proc. IEEE Visualization 2003* (2003), pp. 225–232.

[WJE01] WESTERMANN R., JOHNSON C., ERTL T.: Topology-preserving smoothing of vector fields. *IEEE Transactions on Visualization and Computer Graphics 7*, 3 (2001), 222–229.

[WS01] WISCHGOLL T., SCHEUERMANN G.: Detection and visualization of closed streamlines in planar flows. *IEEE Transactions on Visualization and Computer Graphics 7*, 2 (2001), 165–172.

[WTHS04] WEINKAUF T., THEISEL H., HEGE H.-C., SEIDEL H.-P.: Boundary switch connectors for topological visualization of complex 3d vector fields. In *Data Visualization 2004. Proc. VisSym 04* (2004).

[ZSH96] ZÖCKLER M., STALLING D., HEGE H.: Interactive visualization of 3D-vector fields using illuminated stream lines. In *Proc. IEEE Visualization '96* (1996), pp. 107–113.